Frequency-domain Channel Estimation Using FFT/IFFT for DS-CDMA Mobile Radio

Shinsuke Takaoka and Fumiyuki Adachi
Electrical and Communication Engineering, Graduate School of Engineering, Tohoku University, Japan
05 Aza-Aoba, Aramaki, Aoba-ku, Sendai, 980-8579 Japan
E-mail: takaoka@mobile.ecei.tohoku.ac.jp, adachi@ecei.tohoku.ac.jp

Summary: Coherent rake reception of direct sequence code division multiple access (DS-CDMA) signals requires accurate channel estimation in a frequency-selective fading channel. This paper studies a code-multiplexed pilot-assisted frequency-domain channel estimation using FFT/IFFT, which has a good tracking capability against fast fading and can reduce the effect of noise and interpath interference (IPI). The average bit error rate (BER) performance of rake combining in a time- and frequency-selective fading channel is theoretically evaluated and confirmed by computer simulation. It is shown that the frequency-domain channel estimation using code-multiplexed pilot is very robust against fast fading.

1. Introduction

Direct sequence code division multiple access (DS-CDMA) is used in present cellular mobile communications systems [1]. For coherent rake reception of DS-CDMA signals, accurate channel estimation is necessary and so far many pilot-assisted channel estimation schemes have been studied [2]-[6]. There are two different types of pilot multiplexed structure, i.e., time-multiplexed pilot and code-multiplexed pilot, for the channel estimation [7,8]. Time-multiplexed pilot-assisted channel estimation called weighted multi-slot averaging (WMSA) channel estimation using a finite impulse response (FIR) filter was proposed in [6]. WMSA channel estimation has been shown to provide a good bit error rate (BER) performance for a slow fading. However, the BER performance significantly degrades for fast fading due to the time-invariant FIR filter. Hence, adaptive channel estimation schemes were proposed in [8]-[10]. Code-multiplexed pilot-assisted channel estimation is also attractive since the pilot symbol is continuously transmitted and has a good tracking capability against fast fading. In order to reduce the effect of noise and interpath interference (IPI), an FIR filter can be applied. However, since the FIR filter tap weights need to be changed according to changes in the propagation environment in order to obtain a better channel estimation, some adaptive technique is necessary [8].

All of the above-mentioned channel estimation schemes employ the time-domain processing. Frequency-domain channel estimation using fast Fourier transform (FFT) and zero padding was proposed for a time-multiplexed pilot structure [11]. Since this scheme is equivalent to the time-domain interpolation technique using the sinc function, the noise reduction is not sufficient. DS-CDMA channels are frequency-selective and a large IPI is produced. The IPI must be suppressed for accurate channel estimation. In this paper, we apply a frequency-domain channel estimation using FFT/IFFT to a code-multiplexed pilot structure, which has a good tracking capability against fast fading and can reduce the effect of noise and IPI.

The remainder of this paper is organized as follows. Sect. 2 describes the frequency-domain channel estimation using code-multiplexed pilot for coherent rake reception of DS-CDMA signals. Then, the theoretical analysis of the conditional BER for a given set of the path gains is presented in Sect. 3. In Sect. 4 the theoretical average BER performance is evaluated by Monte-Carlo numerical computation method using the derived BER expression and is confirmed by computer simulation. Sect. 5 offers some conclusions.

2. Frequency-domain Channel Estimation Using FFT/IFFT

Figure 1 shows the receiver structure with frequency-domain channel estimation. We consider the detection of N data symbols in the m-th frame as shown in Fig. 2. For frequency-domain channel estimation, an interval of N_F symbols, which includes the m-th frame in the center, is considered.

2.1 Received Signal Representation

At the transmitter, the quadrature phase shift keying (QPSK) modulated data sequence is spread using orthogonal spreading code with spreading factor SF to obtain the chip sequence and then pilot chip sequence spread by different orthogonal spreading code is code-multiplexed. Finally, the code-multiplexed chip sequence is multiplied by the long scramble code to produce the transmit DS-CDMA signal, which is transmitted over an L-path fading channel. At a receiver, the received DS-CDMA signal is passed through a filter matched to the spreading code sequence in order to resolve the received multipath signal into L signal components having different time delays. The L resolved signals are coherently combined by multiplying the complex conjugates of channel estimates to be data detected.

The received signal can be represented, using the equivalent lowpass representation, as

$$r(t) = \sum_{l=0}^{L-1} \xi_l(t) s(t-\tau_l) + v(t) \tag{1}$$

with

$$s(t) = \sqrt{\frac{2S}{1+Q}} d(t) c_d(t) + \sqrt{\frac{2SQ}{1+Q}} p(t) c_p(t), \tag{2}$$

where $s(t)$, $d(t)$ and $p(t)$ are the transmitted DS-CDMA signal, QPSK modulated data symbol and pilot symbol, respectively. $c_d(t)$ and $c_p(t)$ are the composite spreading waveforms of orthogonal code and long scramble code for the data and pilot symbols. S and Q are the total transmit power and the pilot-to-data power ratio, respectively. $v(t)$ is the background additive white Gaussian noise (AWGN) with one-sided power spectrum density N_0. ξ_l(t) and τ_l are the path gain and time delay of the l-th path, respectively. We assume $\sum_{l=0}^{L-1} E[|\xi_l(t)|^2] = 1$; E[·] denotes the ensemble average operation.

The matched filter (MF) output at the n-th symbol time epoch of the m-th frame, associated with the l-th path, is represented as

$$\begin{cases} \hat{\eta}_l(m,n) = \dfrac{1}{T_s}\displaystyle\int_{mNT_s+nT_s+\tau_l}^{mNT_s+(n+1)T_s+\tau_l} r(t)c_d^*(t-\tau_l)dt \\ \quad = \sqrt{\dfrac{2S}{1+Q}}\xi_l(m,n)d(m,n) + \mu_l^{(d)}(m,n) \quad \text{for data} \\ \hat{\xi}_l(m,n) = \dfrac{1}{T_s}\displaystyle\int_{mNT_s+nT_s+\tau_l}^{mNT_s+(n+1)T_s+\tau_l} r(t)c_p^*(t-\tau_l)dt \\ \quad = \sqrt{\dfrac{2SQ}{1+Q}}\xi_l(m,n)d_p + \mu_l^{(p)}(m,n) \quad \text{for pilot} \end{cases}, \tag{3}$$

where $\xi_l(m,n) = \xi_l(mNT_s + nT_s - (N_F - N)T_s/2)$, $\mu_l^{(d \text{ or } p)}(m,n)$ represents the noise plus IPI component, and * denotes the complex conjugation. A total of L MF outputs are coherently summed up based on maximal ratio combining (MRC) in the rake combiner. The rake combiner output $\eta(m,n)$, which is the decision variable for the data symbol $d(m,n)$, is given by

$$\eta(m,n) = \sum_{l=0}^{L-1} \hat{\eta}_l(m,n)\tilde{\xi}_l^*(m,n) , \tag{4}$$

where $\tilde{\xi}_l(m,n)$ is the estimate of $\xi_l(m,n)$.

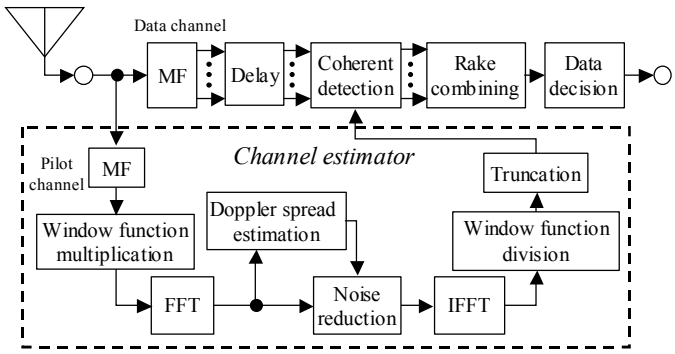

Fig. 1 Receiver structure.

2.2 Frequency-domain Channel Estimation

First, the instantaneous path gains $\{\hat{\xi}_l(m,n); l = 0 \sim L-1, n = 0 \sim N_F - 1\}$ over the m-th frame of length N symbols are estimated using MF output for the pilot symbol in Eq. (3). Assuming d_p=1+j0 without loss of generality, the instantaneous path gain $\hat{\xi}_l(m,n)$ given by Eq. (3),

$$\hat{\xi}_l(m,n) = \sqrt{\frac{2SQ}{1+Q}}\xi_l(m,n) + \mu_l^{(p)}(m,n) , \tag{5}$$

is multiplied by the window function $w(n)$ and the N_F-point FFT is carried out to obtain

$$\hat{H}_l(m,k) = \sum_{n=0}^{N_F-1} \hat{\xi}_l(m,n)w(n)\exp\left(-j2\pi\frac{n}{N_F}k\right) \tag{6}$$

for k=0~N_F-1. Remembering that the frequency components of the AWGN and IPI are uniformly distributed over whole frequency band, k=0~N_F-1, while that of the fading path gain is bandlimited to the maximum Doppler frequency f_D, we replace the components of frequencies above f_D by zero's to suppress the contribution from AWGN and IPI:

$$\tilde{H}_l(m,k) = \begin{cases} \hat{H}_l(m,k), & 0 \le k < N_D + \alpha \\ & \text{and } N_F - (N_D + \alpha) \le k < N_F \\ 0 & \text{, elsewhere} \end{cases}, \tag{7}$$

where N_D corresponds to the maximum Doppler frequency and α is the Doppler margin. Then, the time-domain channel estimate is obtained by applying the N_F-point IFFT as

$$\tilde{\xi}_l(m,n) = \frac{1}{w(n)N_F}\sum_{k=0}^{N_F-1}\tilde{H}_l(m,k)\exp\left(j2\pi\frac{k}{N_F}n\right) \tag{8}$$

for n=0~N_F-1. Finally, we pick up $\tilde{\xi}_l(m,n)$'s, (N_F - N)/2≤ n ≤(N_F + N)/2-1, in the center region of N symbols to avoid the noise enhancement and the alias effect. Using the estimated channel gains, coherent L-finger rake combining of Eq. (4) is carried out, followed by the data demodulation of the m-th frame.

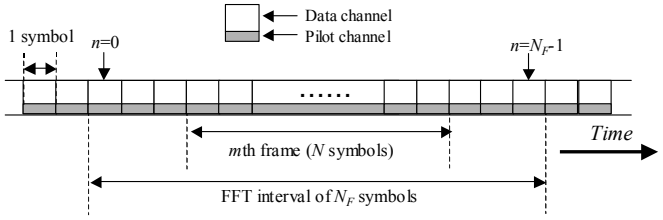

Fig. 2 Channel estimation interval.

2.3 Maximum Doppler Frequency Estimation

Code-multiplexed pilot-assisted frequency-domain channel estimation requires the knowledge of the maximum Doppler frequency. The instantaneous fading power spectrum of the l-th path gain is given by

$$\hat{P}_l(m,k) = \left|\hat{H}_l(m,k)\right|^2 \quad \text{for } k = 0 \sim N_F - 1 , \tag{9}$$

which is corrupted by the AWGN and IPI components. Since $\hat{P}_l(m,k) = \hat{P}_l(m,N_F - k)$ and assuming that each path has the same maximum Doppler frequency, simple frequency-domain averaging is first carried out as

$$\tilde{P}(m,k) = \frac{1}{2L}\sum_{l=0}^{L-1}\left\{\hat{P}_l(m,k) + \hat{P}_l(m,N_F - k)\right\} \tag{10}$$

for k=0~N_F/2-1. Then, time-domain averaging is carried out using a first order linear filter as

$$\overline{P}(m,k) = \beta\overline{P}(m-1,k) + (1-\beta)\tilde{P}(m,k) , \tag{11}$$

where β (<1) is the forgetting factor and $\overline{P}(0,k) = \tilde{P}(0,k)$. Finally, we search for the frequency position having the peak power as

$$N_D = \underset{k=0\sim N_F/2-1}{\arg\max}\ \overline{P}(m,k) , \tag{12}$$

which is used in Eq. (7).

3. Theoretical BER Analysis

The noise plus IPI component $\mu_l^{(p)}(m,n)$ in the

instantaneous path gain $\hat{\xi}_l(m,n)$ in Eq. (5) is modeled as a zero-mean complex-valued Gaussian noise. The conditional BER is derived for a given set of the path gains $\{\xi_l(m,n)\}$. In the following derivation, we assume that a receiver has the perfect knowledge of the maximum Doppler frequency, i.e., N_D.

After the frequency-domain channel estimation described in Sect. 2.2 is carried out, we obtain the final channel estimate $\tilde{\xi}_l(m,n)$. Assuming that the frequency component of the windowed fading path gain is bandlimited to the maximum Doppler frequency f_D, Eq. (8) can be approximately given by

$$\tilde{\xi}_l(m,n) \approx \sqrt{\frac{2SQ}{1+Q}}\xi_l(m,n) + \Pi_l^{(p)}(m,n), \tag{13}$$

where $\Pi_l^{(p)}(m,n)$ is the residual AWGN plus IPI component. The variance of $\mu_l^{(p)}(m,n)$ is given by

$$2\sigma_\mu^2 = 2\left(\frac{N_0}{T_s}\right)\left\{\left(\frac{E_s}{N_0}\right)\frac{1}{SF}\sum_{\substack{l'=0\\ \neq l}}^{L-1}\left|\xi_{l'}(m,n)\right|^2 + 1\right\}, \tag{14}$$

where E_s (=$2E_b$) and T_s are the QPSK symbol energy and symbol length. Therefore, the variance of $\Pi_l^{(p)}(m,n)$ can be given by

$$2\sigma_\Pi^2 = \frac{4\left(\frac{N_0}{T_s}\right)}{w^2(n)N_F^2}(N_D+\alpha) \times \sum_{n'=0}^{N_F-1}\left\{\left(\frac{E_s}{N_0}\right)\frac{1}{SF}\sum_{\substack{l'=0\\ \neq l}}^{L-1}\left|\xi_{l'}(m,n')\right|^2 + 1\right\}w^2(n'). \tag{15}$$

The data symbol $d(m,n)$ is to be detected. The noise plus IPI component $\mu_l^{(d)}(m,n)$ in the MF output $\hat{\eta}_l(m,n)$, given by Eq. (3), can be expressed as

$$\mu_l^{(d)}(m,n) = \sum_{\substack{l'=0\\ \neq l}}^{L-1}\xi_{l'}(m,n)\frac{1}{T_s}\int_0^{T_s}\left(\begin{array}{l}\sqrt{\frac{2S}{1+Q}}d(t-\tau_l)q_{d,d}(t;l,l') \\ +\sqrt{\frac{2SQ}{1+Q}}p(t-\tau_l)q_{p,d}(t;l,l')\end{array}\right)dt + v_l(m,n), \tag{16}$$

where

$$\begin{cases} q_{p,d}(t;l,l') = c_p(t-\tau_l)c_d^*(t-\tau_{l'}) \\ q_{d,d}(t;l,l') = c_d(t-\tau_l)c_d^*(t-\tau_{l'}) \end{cases}. \tag{17}$$

The first term of Eq. (16) represents the sum of the IPI for data symbol and the second term $v_l(m,n)$ is a complex Gaussian noise sample with the variance of $2N_0/T_s$. Following the same procedure as in [12], the IPI is modeled as a complex Gaussian noise and combined with the AWGN.

Using Eqs. (4) and (13), the desired signal power of the rake combiner output $\eta(m,n)$ is given by

$$P \approx 2\left(\frac{E_s}{T_s}\right)^2\frac{Q}{(1+Q)^2}\left\{\sum_{l=0}^{L-1}\left|\xi_l(m,n)\right|^2\right\}^2. \tag{18}$$

The composite spreading sequences $q_{p,d}(t;l,l')$ and $q_{d,d}(t;l,l')$ with different time shift randomly take 1 and -1 with equal probability from the nature of long scramble code. Taking this into account, the IPI plus background noise power I in the rake combiner output $\eta(m,n)$ can be approximately given, from Eqs. (4), (13), (15) and (16), by

$$\begin{aligned} I \approx{}& 2\left(\frac{N_0}{T_s}\right)\left(\frac{E_s}{T_s}\right)\frac{Q}{1+Q}\sum_{l=0}^{L-1}\left|\xi_l(m,n)\right|^2\left\{\left(\frac{E_s}{N_0}\right)\frac{1}{SF}\sum_{\substack{l'=0\\ \neq l}}^{L-1}\left|\xi_{l'}(m,n)\right|^2 + 1\right\} \\ &+ \frac{4\left(\frac{N_0}{T_s}\right)^2}{w^2(n)N_F^2}(N_D+\alpha) \\ &\times \sum_{l=0}^{L-1}\left[\left(\frac{E_s}{N_0}\right)\frac{Q}{1+Q}\left|\xi_l(m,n)\right|^2 + \left(\frac{E_s}{N_0}\right)\frac{1}{SF}\sum_{\substack{l'=0\\ \neq l}}^{L-1}\left|\xi_{l'}(m,n)\right|^2 + 1\right] \\ &\times \left[\sum_{n'=0}^{N_F-1}\left\{\left(\frac{E_s}{N_0}\right)\frac{1}{SF}\sum_{\substack{l'=0\\ \neq l}}^{L-1}\left|\xi_{l'}(m,n')\right|^2 + 1\right\}w^2(n')\right] \end{aligned}. \tag{19}$$

Hence, the conditional BER of the n-th symbol position in a frame for a given set of path gains $\{\xi_l(m,n)\}$ can be given by

$$P_b^{(n)}\left(\frac{E_s}{N_0}, \{\xi_l(m,n)\}\right) = \frac{1}{2}erfc\left(\sqrt{\frac{P}{2I}}\right) \tag{20}$$

for QPSK, where $erfc(x) = (2/\sqrt{\pi})\int_x^\infty \exp(-t^2)dt$ is the complementary error function. The theoretical average BER of the n-th symbol position in a frame can be numerically evaluated by averaging Eq. (20) over $\{\xi_l(m,n)\}$:

$$P_b^{(n)}\left(\frac{E_s}{N_0}\right) = \int\cdots\int\frac{1}{2}erfc\left(\sqrt{\frac{S}{2I}}\right)p(\{\xi_l(m,n)\})\prod_l d\{\xi_l(m,n)\}, \tag{21}$$

where $p(\{\xi_l(m,n)\})$ is the joint probability density function (pdf) of $\{\xi_l(m,n)\}$. Then, the average BER over one frame is obtained by

$$P_b\left(\frac{E_s}{N_0}\right) = \frac{1}{N}\sum_{n=(N_F-N)/2}^{(N_F+N)/2-1}P_b^{(n)}\left(\frac{E_s}{N_0}\right). \tag{22}$$

4. Numerical and Simulation Results

The numerical evaluation of the theoretical average BER is done by Monte-Carlo numerical computation method as follows. The set of path gain $\{\xi_l(m,n)\}$ is generated and then the conditional BER of the n-th symbol position in a frame for the given symbol

energy E_s/N_0 and $\{\xi_l(m,n)\}$ is computed using Eq. (20). This is repeated sufficient number of times to obtain the theoretical average BER of Eq. (21). Computer simulation parameters are summarized in Table 1. A T_c-spaced L=4-path frequency-selective Rayleigh fading channel having a uniform power delay profile, i.e., $E[|\xi_l(m,n)|^2]=1/L$ is assumed. Data modulation and spreading modulation are QPSK and BPSK, respectively.

Table 1 Simulation condition.

Transmitter	Spreading factor	64	
	Modulation	Data	QPSK
		Spreading	BPSK
	Orthogonal code	Walsh code	
	Scramble code	Long PN sequence	
Channel model	Rayleigh fading with 4-path uniform power delay profile		
Receiver	Diversity	4-finger rake	
	Frame length	N=256	
	Window function	Hanning window	
	Doppler margin	α=2	
	Forgetting factor	β=0.95	

Since channel estimation accuracy depends on pilot power ratio Q, the selection of Q is important. As Q increases, the SINR of the instantaneous path gain estimates $\{\hat{\xi}_l(m,n)\}$ in Eq. (5) improves. Accordingly, the BER performance improves. However, the transmission of non-information bearing pilot symbols degrades the BER performance due to the increase in power loss. Hence, first, we evaluate how the pilot power ratio Q affects the average BER performance. Fig. 3 plots the theoretical average BER performances as a function of the average received E_b/N_0 with Q as a parameter for f_DT_s=0.004 and N_F=512. We set N_D=3 in the numerical evaluation of the theoretical average BER due to $(f_DT_s)/(1/2)$x(512/2)=2.048. In Fig. 3, the simulation results are also plotted for comparison with theoretical result. The theoretical and simulated BER performances are in good agreement. This confirms the validity of the maximum Doppler frequency estimation described in Sect. 2.3. It is found that BER decreases as Q increases; however, the excessive pilot power degrades the BER performance due to the power loss. From Fig. 3, Q =0.1 was used in the following simulations.

Since the FFT/IFFT is used in channel estimation process, the number N_F of FFT/IFFT points is an important parameter. Reducing N_F reduces the receiver complexity and the processing delay; however, the achievable BER performance may degrade due to the alias effect and the noise enhancement at the beginning and end of the frame. The noise enhancement is caused by the division of the small value of the window function $w(n)$ at the beginning and end of the frame (see Eq. (8)). Fig. 4 plots the average BER performances with L=4 as a function of the average received E_b/N_0 with N_F as a parameter. When N_F=256 (=N), the achievable BER performance significantly degrades since the contribution of the alias effect and the noise enhancement becomes larger. When N_F>512, almost no additional improvement is obtained. Therefore, we used N_F=512 in the following simulation.

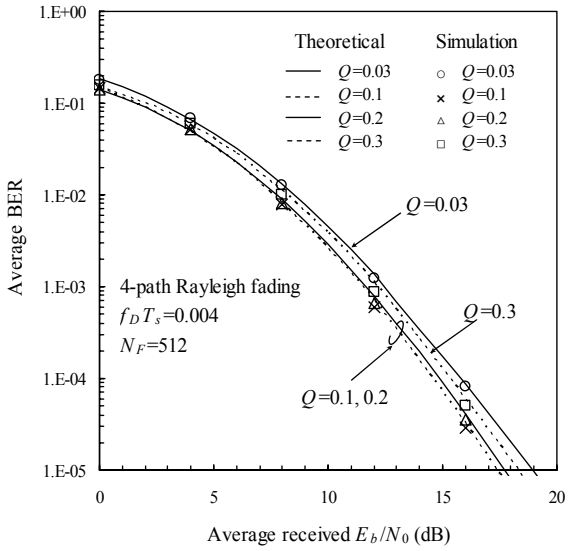

Fig. 3 Effect of Q.

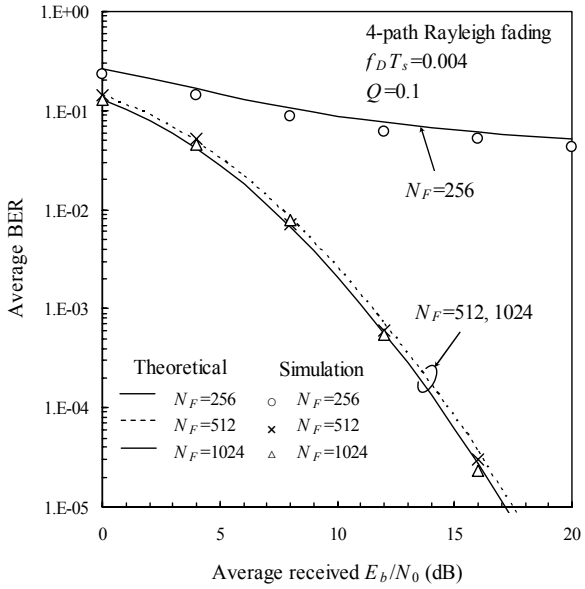

Fig. 4 Effect of N_F.

Next, we compare the average BER performance with the channel estimation scheme using time-multiplexed pilot and that with frequency-domain channel estimation scheme using code-multiplexed pilot by computer simulation. For the conventional channel estimation schemes, we consider FFT channel estimation [11] and K=1- or 2-WMSA channel estimation, both using time-multiplexed pilot (N_p=4 and N_d=36 [6]) (the tap-weight vectors are {1.0, 1.0} and {0.6, 1.0, 1.0, 0.6} for K=1- and 2-WMSA, respectively [6]). Pilot power ratio is Q=0.1. Fig. 5 plots the average BER performances as a function of the average received E_b/N_0 for f_DT_s=0.004. It is seen from Fig. 5 that K=1- and 2-WMSA provide good BER performances in a low E_b/N_0 region, but exhibit error floors in a high E_b/N_0 region since these schemes are designed for reducing the noise effect at the cost of slightly losing the tracking ability against fast fading. FFT channel estimation of Ref. [11] using time-multiplexed pilot provides overall good BER performance in comparison with WMSA since the exact interpolation can be achieved. On the other hand, the

code-multiplexed pilot-assisted frequency-domain channel estimation always provides the best BER performance over all E_b/N_0 regions. The BER improvement from Ref. [11] is due to the sufficient reduction of the AWGN and IPI. The degradation in E_b/N_0 from ideal channel estimation for achieving BER=10^{-4} is as small as 1.0 dB (out of which a 0.46 dB degradation is due to pilot power loss). Fig. 6 plots the simulated average BER performances as a function of the normalized maximum Doppler frequency f_DT_s at average received E_b/N_0=16dB. As f_DT increases, the BER with channel estimation scheme using time-multiplexed pilot rapidly increases. This is because the distortion-free channel estimation is only possible when $f_DT_s \leq 0.0125$ according to the sampling theorem. On the other hand, for the code-multiplexed case, we can achieve a distortion-free channel estimation if $f_DT_s \leq 0.5$ according to the sampling theorem.

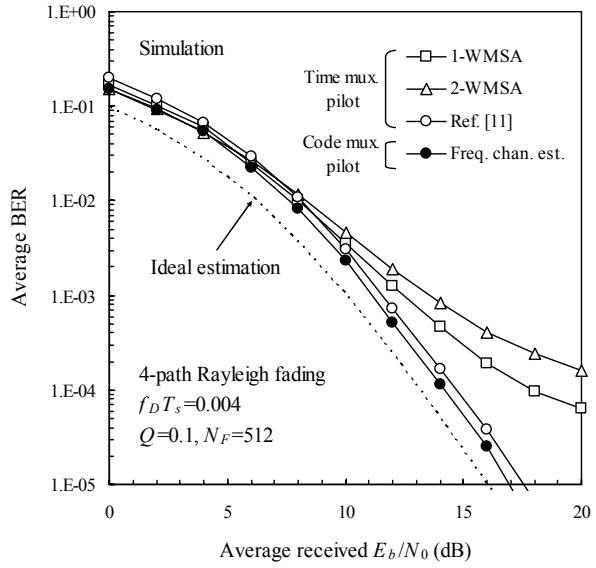

Fig. 5 BER performance comparison.

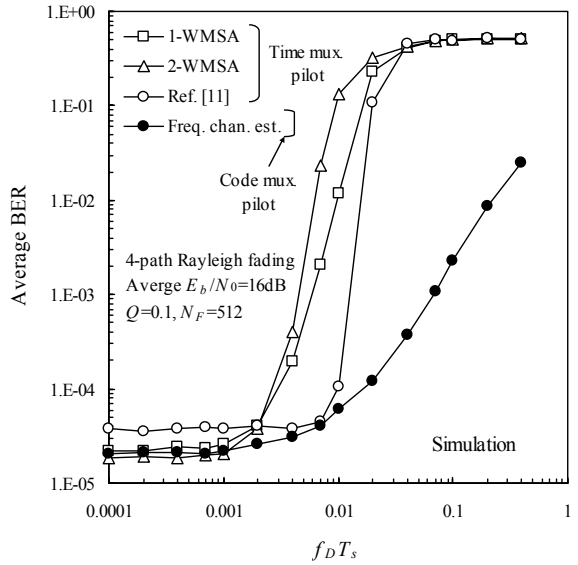

Fig. 6 Effect of fading rate.

5. Conclusion

Code-multiplexed pilot-assisted frequency-domain channel estimation using FFT/IFFT was studied for DS-CDMA rake combining. The average BER performance in a frequency-selective fading channel was theoretically analyzed and confirmed by computer simulation. It was shown that frequency-domain channel estimation using code-multiplexed pilot structure has a good tracking capability against fast fading and provides a superior BER performance to the channel estimation scheme using time-multiplexed pilot.

References

[1] F. Adachi, M. Sawahashi and H. Suda, "Wideband DS-CDMA for next generation mobile communication system," IEEE Commun. Mag., vol. 36, pp. 56-69, Sept. 1998.

[2] J. K. Cavers, "An analysis of pilot symbol assisted modulation for Rayleigh fading channels," IEEE Trans. Veh. Technol., Vol. 40, No. 4, pp. 686-693, Nov. 1991.

[3] F. Ling, "Coherent detection with reference-symbol based estimation for direct sequence CDMA uplink communications," Proc. IEEE Vehicular Tech. Conference, New Jersey, pp. 400-403, May 1993.

[4] Y. Honda and K. Jamal, "Channel estimation based on time-multiplexed pilot symbols," IEICE Technical Report, RCS96-70, pp. 31-35, Aug. 1996.

[5] P. Schramm, "Analysis and optimization of pilot-channel assisted BPSK for DS-CDMA systems," IEEE Trans. Commun., Vol. 46, No. 9, pp. 1122-1124, Sept. 1998.

[6] H. Andoh, M. Sawahashi and F. Adachi, "Channel estimation filter using time-multiplexed pilot channel for coherent rake combining in DS-CDMA mobile radio," IEICE Trans. Commun., Vol. E81-B, pp.1517-1526, July 1998.

[7] S. Abeta, M. Sawahashi and F. Adachi, "Performance comparison between time-multiplexed pilot channel and parallel pilot channel for coherent rake combining in DS-CDMA mobile radio," IEICE Trans. Commun., Vol. E81-B, pp.1417-1425, July 1998.

[8] S. Abeta, M. Sawahashi and F. Adachi, "Adaptive channel estimation for coherent DS-CDMA mobile radio using time-multiplexing pilot and parallel pilot structures," IEICE Trans. Commun., Vol. E82-B, pp.1505-1513, Sept.1999.

[9] S. Takaoka and F. Adachi, "Adaptive prediction iterative channel estimation for combined antenna diversity and coherent rake reception of multipath-faded DSSS signals," IEICE Trans. Commun., Vol. E85-B, No.11, pp. 2405-2415, Nov. 2002.

[10] S. Takaoka and F. Adachi, "Pilot-assisted adaptive channel estimation using multiple sets of tap weights for coherent rake reception of DS-CDMA signals," Proc. 8th CIC2003, pp. 384, Korea, Oct. 2003.

[11] E. Okamoto, H. B. Li and T. Ikegami, "Rayleigh fading compensation for 16QAM using FFT," IEEE Trans. Veh. Tech., Vol. 48, pp. 1626-1633, Sept. 1999.

[12] F. Adachi, "Transmit power efficiency of fast transmit power controlled DS-CDMA reverse link," IEICE Trans. Fundamentals, Vol. E80-A, pp. 2420-2428, Dec. 1997.